CrossMark

J. Fluid Mech. (2017), *vol.* 833, *pp.* 445–468. © Cambridge University Press 2017
doi:10.1017/jfm.2017.718

Path instabilities of oblate spheroids

W. Zhou[1], M. Chrust[2] and J. Dušek[1,†]

[1]ICube, Department of Fluid Mechanics, Université de Strasbourg/CNRS, 2, rue Boussingault, 67000 Strasbourg, France

[2]Earth System Assimilation Section, Data Assimilation Methodology Group, European Centre for Medium-Range Weather Forecasts Shinfield Park, Reading RG2 9AX, UK

(Received 11 January 2017; revised 30 August 2017; accepted 2 October 2017; first published online 6 November 2017)

In the present paper, we investigate the path instabilities and the transition scenario for oblate homogeneous spheroids falling (or ascending) freely in a quiescent and unconfined Newtonian fluid under the action of gravity, buoyancy and hydrodynamic forces. The problem depends on three independent external parameters: the aspect ratio $\chi = d/a$, where d is the diameter and a the length of the axisymmetry axis of the spheroid; the non-dimensionalized mass $m^* = m/(\rho d^3)$, m being the mass of the spheroid and ρ the fluid density; and the Galileo number, defined as $G = \sqrt{(m^* - V^*)gd^3}/\nu$. In the definition of the Galileo number, $V^* = V/d^3$ is the non-dimensionalized volume, g the gravitational acceleration and ν is the kinematic viscosity. Asymptotic solutions (regimes) are investigated in seven $\chi = \text{const.}$ parameter planes going from $\chi = 10$ (very flat spheroid) to $\chi = 1.1$ (an almost spherical shape), for m^* going from 0 to 5 and Galileo numbers up to 300 (i.e. Reynolds numbers roughly up to 500). The obtained results provide a link between the known scenario of a homogeneous disk and that, well known, of a sphere. The scenario of the flat spheroid of aspect ratio 10 has many common features with that of an infinitely thin disk, but the finite thickness brings about significant quantitative differences. At the opposite side of the investigated aspect ratio interval, the dynamics of the spheroid of aspect ratio 1.1 is found very close to that of a perfect sphere except for small density ratios (smaller than approximately 0.5). Very light spheroids of aspect ratio 1.1 move along vertical zig-zagging trajectories. At intermediate aspect ratios, the strong subcritical effects and the characteristic zig-zagging and fluttering motion, typical for flat bodies, progressively disappear. The tumbling regime remains remarkably stable and is shown to be present down to $\chi = 2$. An interesting result consists in the evidence of the first two bifurcations typical for the sphere scenario (leading to steady oblique and oblique oscillating trajectories) present both for very flat and thick spheroids but absent at intermediate aspect ratios. The results pertaining to spheroids might be more useful in practical applications than those obtained for too idealized thin disks and perfect spheres.

Key words: multiphase and particle-laden flows, particle/fluid flow, wakes

† Email address for correspondence: dusek@unistra.fr

https://doi.org/10.1017/jfm.2017.718 Published online by Cambridge University Press

1. Introduction

Multi-particle flows have many applications in industrial and environmental problems, such as sedimentation and erosion, chemistry (fluidized beds), combustion, biology and medical science. The behaviour of multi-particle flows depends on many factors, such as the turbulence, particle–particle interaction and own particle dynamics acting on very different scales. This makes numerical multi-particle multi-scale models extremely complex and dependent on the advancement of knowledge of all involved phenomena. The individual particle dynamics can, under some conditions, have a very significant impact on a multi-particle flow behaviour. A recent work by Uhlmann & Doychev (2014) demonstrated this fact in the case of sedimentation of a dilute system of spherical particles. It established a clear relation between the onset of path instabilities of freely falling spheres and the formation of sedimentation clusters. Path instabilities have, however, much larger effects on the dynamics of rather flat bodies than spheres. The review paper by Ern *et al.* (2011) sums up the knowledge on path instabilities of simple, homogeneous, mostly axisymmetric or two-dimensional (2D), bodies such as disks, flat cylinders, spheroids and 2D plates, based on experimental observations and numerical simulations by the beginning of the present decade.

More recent results brought significant progress in understanding the transition scenario of very flat or even nominally infinitely flat bodies, and also knowledge of the scenario of perfect homogeneous spheres has been improved. As for perfect homogeneous spheres, a finer linear and weakly nonlinear analysis of the first two bifurcations was provided by Fabre, Auguste & Magnaudet (2008) and Fabre, Tchoufag & Magnaudet (2012). Benchmarking of interface-resolved multi-particle flow simulations at significant particle Reynolds numbers (see Uhlmann & Dušek 2014) stimulated an interest in more accurate data and for a better understanding of chaotic trajectories (Zhou & Dušek 2015). From the mathematical viewpoint, the problem can be parametrized by two non-dimensional external parameters, the Galileo number, defined as $G^* = \sqrt{|\rho_s/\rho - 1|gd^3}/\nu$, and the density ratio ρ_s/ρ, where ρ and ρ_s are, respectively, the density of the fluid and of the solid, d the diameter of the sphere, g the gravitational acceleration and ν the kinematic viscosity of the fluid. (The '$*$' in the notation G^* has been introduced here to distinguish the definition used in the context of a perfect sphere, e.g. in papers by Jenny, Dušek & Bouchet (2004), Zhou & Dušek (2015), Uhlmann & Dušek (2014), from that introduced to account for more general shapes by Chrust, Bouchet & Dušek (2013) and used in the present paper.) As confirmed by all the cited work, the two primary bifurcating states are characterized by steady oblique and oblique oscillating trajectories. Fabre *et al.* (2012) showed that the primary instability threshold is independent of the density ratio. There is wide consensus that the critical Galileo number is 156. The linear analysis of Tchoufag, Fabre & Magnaudet (2014) pointed out the theoretical existence of modes with strong and weak solid–fluid interaction called, respectively, solid and fluid modes. Our recent paper (Zhou & Dušek 2015) put this theoretical result in relation with the existence of two different frequencies of oblique oscillating trajectories remarked already by Jenny *et al.* (2004). A similar scenario has been predicted also for flat cylinders by Tchoufag *et al.* (2014). In what follows, a sequence of a steady oblique and an oblique oscillating state will be called sphere scenario.

Flat bodies are known to present far more spectacular path instabilities than spheres. The, by now already classical, results (Willmarth, Hawk & Harvey 1964; Stringham, Simons & Guy 1969; Field, Klaus & Moore 1997) describing experimental observations of the fall of thin disks have been commented upon in the review paper by Ern *et al.* (2011). Additional important experimental data is due to Fernandes *et al.*

https://doi.org/10.1017/jfm.2017.718 Published online by Cambridge University Press

(2007) and Zhong, Chen & Lee (2011). Ern *et al.* (2011) sum up the observations into four categories of regimes (of non-vertical trajectories): A – mostly chaotic with small amplitude of oscillation, B and C – period harmonic or anharmonic, oscillating along a mean vertical direction with planar or helical trajectories, and D – highly 'nonlinear', i.e. chaotic and strongly oscillating. This list is to be completed by the 'tumbling' regime of Field *et al.* (1997). The experimental data are classically parametrized by the Reynolds number based on the mean vertical velocity and by the non-dimensionalized moment of inertia $I^* = I/(\rho d^5)$ (I being the moment of inertia with respect to an axis lying in the plane of the disk). Each trajectory type is associated with a specific subset of the parameter plane represented in a state diagram.

The experiments of Field *et al.* (1997) stimulated a significant effort to develop an appropriate simulation method capable of reproducing the observations with sufficient accuracy at acceptable costs to allow a parametric study. The challenge of reproducing the experiments was raised by two theses: that by Auguste (2010) and by Chrust (2012). Auguste (2010) (see also Auguste, Magnaudet & Fabre 2013) showed the existence of small-amplitude non-vertical regimes preceding the appearance of large planar oscillations of very flat cylinders. These trajectories, experimentally hard to distinguish from vertical ones, were conjectured to explain the surprising observation of Fernandes *et al.* (2007). A recent paper by Chrust, Bouchet & Dušek (2014) confirmed this conjecture quantitatively. Similarly as for spheres, the weakly oscillating regime represents a fluid mode while all the easily observable regimes are solid modes. Chrust *et al.* (2013) present a numerical counterpart of the experiments by Field *et al.* (1997) by investigating the transition scenario of thin disks of infinite nominal aspect ratio χ and of variable inertia. Instead of I^*, the disk inertia is characterized by the non-dimensionalized mass $m^* = m/(\rho d^3)$, where ρ is the fluid density, d the disk diameter and m its mass. Instead of the Reynolds number based on an *a priori* unknown vertical velocity, the Galileo number is defined as

$$G = \sqrt{|m^* - V^*|gd^3}/\nu, \tag{1.1}$$

where $V^* = V/d^3$ is the non-dimensionalized volume (accounting for buoyancy in the definition (1.1)) and ν the kinematic viscosity of the fluid. A good agreement with experiments was obtained and, moreover, many additional facts were revealed. Most notable were the strong subcritical effects leading to coexistence of stable states and a substantially different scenario for light ($m^* < 1$) and massive ($m^* > 1$) disks. It is interesting to note that the above-mentioned fluid modes, observed as weakly oscillating periodic and chaotic states filling a gap between the loss of stability of the vertical fall and the onset of instability of a strong flutter in the same manner as for flat cylinders, were evidenced only for very small non-dimensionalized masses $m^* < 0.1$. At $m^* = 0$, the critical Galileo number for loss of stability of the vertical fall was found to be $G = 78$ and strong flutter was evidenced starting only from $G = 130$. Moreover, again at $m^* = 0$, the chaotic weakly oscillating state was found to coexist with the strong periodic flutter in the wide interval $130 \leqslant G \leqslant 180$. The virtually experimentally unobservable, weakly oscillating states were shown to explain the shape of the critical curve of Willmarth *et al.* (1964) characterized by a strong upward shift of the observed onset of oscillations (flutter) of very light disks. The planar periodically zig-zagging, intermittent and tumbling trajectories were shown to become spiral at higher Galileo numbers. In particular, the spiral trajectories of Zhong *et al.* (2011) were evidenced for small non-dimensionalized masses.

https://doi.org/10.1017/jfm.2017.718 Published online by Cambridge University Press

The comparison of the state diagrams figure 3 of Zhou & Dušek (2015) and figure 22 of Chrust *et al.* (2013) shows no obvious analogy between the scenario of spheres and disks. Since various flat objects of intermediate aspect ratio occur in many applications of multi-particle flows, the question of the behaviour of particles of intermediate shape may be of interest. Chrust, Bouchet & Dušek (2010) motivated the use of a family of spheroids of variable aspect ratio for establishing the link between the transition scenario of an infinitely flat disk and a sphere by the possibility of parametrizing all intermediate shapes continuously by a single parameter – the aspect ratio defined as $\chi = d/a$, where d is the diameter and a the length of the axisymmetry axis of the spheroid. In the present paper, we aim to establish this link for freely moving bodies under the action of gravity, buoyancy and hydrodynamic forces. The limit cases are represented by a spheroid of infinite aspect ratio and an imperfect sphere. Neither corresponds exactly to the idealized bodies, for which the path instabilities have been investigated in much detail. While the fact that the limit of infinite aspect ratio of a homogeneous spheroid does not have a uniform mass distribution, and thus its non-dimensional moment of inertia is $m^*/20$ instead of $m^*/16$, is relatively inessential; the limit towards $\chi = 1$ does not converge to a perfect sphere since it does not allow a free rotation. This has a significant impact on the behaviour of very light bodies. Seven intermediate aspect ratios ranging from 10 to 1.1 are considered.

2. Mathematical formulation and numerical method

The mathematical formulation is described in the paper by Chrust *et al.* (2013). Here, we sum up the main features. The fluid is assumed to be incompressible with constant density ρ and Newtonian with constant kinematic viscosity ν. The motion of a homogeneous rigid spheroid, of diameter d and the length of the polar axis a, is driven by gravity and buoyancy. To keep the link with the thin disc of Chrust *et al.* (2013), we characterize the inertia by the non-dimensionalized mass whereas the buoyancy effect is given by the non-dimensionalized volume:

$$m^* = \frac{m}{\rho d^3}, \quad V^* = \frac{V}{d^3}. \tag{2.1a,b}$$

The flow and solid-body equations are then non-dimensionalized using the velocity scale

$$U_{ref} = \sqrt{|m^* - V^*|gd}. \tag{2.2}$$

The velocity scale U_{ref} and length scale d are used to non-dimensionalize all other quantities, such as the time, frequency, vorticity etc., appearing throughout this. This non-dimensionalization must be taken into account for conversion to/from physical units.

A very thin spheroid of finite mass m can be considered to be made of an infinitely dense material and to have a zero volume. From this viewpoint, the buoyancy effects would be negligible, as is the case for experiments in the air. In water, however, the solid/fluid density ratio (ρ_s/ρ) remains small and buoyancy combined with gravity results in an effective gravitational acceleration $g_{eff} = (1 - \rho/\rho_s)g$, where g is the gravitational acceleration. The definition of g_{eff} covers both falling and ascending spheroids. The present velocity scale differs by the factor $\sqrt{V^*} = \sqrt{\pi/6}$ from that used, in general, for the simulation of freely moving spheres (e.g. in Jenny *et al.*

https://doi.org/10.1017/jfm.2017.718 Published online by Cambridge University Press

Parameter	Meaning	Definition
d	Diameter	
a	Length of symmetry axis	
χ	Aspect ratio	$\chi = d/a$
$\rho,\ \rho_s$	Fluid and solid density	
g	Gravitational acceleration	
V^*	Non-dimensionalized volume	$V^* = V/d^3 = \pi/(6\chi)$
m^*	Non-dimensionalized mass	$m^* = m/(\rho d^3) = \rho_s V^*/\rho$
α	Ratio of principal inertial moments	$\alpha = I_z/I = 2\Big/\left(1+\dfrac{1}{\chi^2}\right)$
G	Galileo number	$G = \sqrt{\lvert m^* - V^*\rvert g d^3}/\nu$

TABLE 1. Used parameters.

2004). The fluid is assumed to adhere perfectly to the solid-body surface. The fluid medium is considered infinite and quiescent far from the moving body.

The fluid and solid-body equations have exactly the same form as in Chrust *et al.* (2013). The non-dimensionalized viscosity is given by the inverse of the Galileo number defined as:

$$G = \frac{U_{ref} d}{\nu} = \frac{\sqrt{|m^* - V^*|gd^3}}{\nu} = \frac{\sqrt{m^* g_{eff} d^3}}{\nu}. \tag{2.3}$$

The aspect ratio χ appears in the expressions for the non-dimensionalized volume V^*, mass m^*, moment of inertia I^* and the ratio $\alpha = I_z/I$ where I_z and I are the moment of inertia with respect to the axisymmetry axis and to a perpendicular axis, respectively. The corresponding expressions can be written as:

$$V^* = \frac{\pi}{6\chi}, \quad m^* = \frac{\rho_s}{\rho} V^*, \quad I^* = m^* \left(1 + \frac{1}{\chi^2}\right) \Big/ 20, \quad \alpha \equiv \frac{I_z}{I} = \frac{2}{1 + \dfrac{1}{\chi^2}}. \tag{2.4a–d}$$

As can be seen, G, m^* and χ represent three independent parameters fully paramerizing the problem. Alternatively, for example, the density ratio could be used instead of the non-dimensionalized mass provided the infinite aspect ratio were not considered. The essential parameters are summed up in table 1.

The numerical method consists in a domain decomposition of a cylindrical vertical domain, accompanying the translation motion, into a small spherical subdomain rotating with the solid body and the remaining cylindrical domain keeping a vertical axis. For the schematic of the numerical domain and more details, the reader is invited to refer to the paper by Chrust *et al.* (2013). The fully implicit fluid–solid coupling described in Jenny & Dušek (2004) allows us to account with the same accuracy and costs for bodies of any, especially of small, inertia. The spatial discretization consists in a spectral azimuthal Fourier expansion combined with a spectral element decomposition in the axial–radial plane in both subdomains. The axis of the spherical subdomain coincides with that of the spheroid. A practically identical spectral element mesh as in Chrust *et al.* (2013) is used. Since the axes of the two subdomains are not aligned, the connection is provided by a spherical function decomposition on

https://doi.org/10.1017/jfm.2017.718 Published online by Cambridge University Press

the spherical interface of radius $R_s = 1d$. The classical rotation matrices yield a highly efficient way how to implement the rotations. The technical details of the numerical method can be found in the PhD thesis by Chrust (2012). The numerical testing was performed for a light sphere by comparison to the code without domain decomposition, for a disk by comparison to results of Auguste (2010), as well as for a cylinder of aspect ratio 1 (by testing the sensitivity of critical Galileo numbers to numerical parameters). The retained numerical mesh and a truncation of the azimuthal and spherical function expansions, at $M = 15$ and $\ell_{max} = 15$ were shown to assure an excellent accuracy of approximately 0.1 in terms of the critical Galileo number of the primary instability thresholds, as well as the secondary ones, for the sphere and cylinder.

3. Results

The transition scenario of freely falling or ascending spheroids is characterized by a set of bifurcating asymptotic states. They correspond to stable asymptotic regimes reached in an infinite time horizon by the solid–fluid system for a fixed set of state parameters. In practical situations, 'infinite' means extremely diverse time scales given by the stability of the state. The latter decreases dramatically close to bifurcations and at the onset of chaos. Given the objective to detect asymptotic states, the initial conditions of the simulations are to a great extent arbitrary. They are chosen using already known results. This allows us not only to save CPU time but it is the only practical way how to track branches of coexisting solutions in the many cases of subcritical bifurcations that occur in our study.

This section is organized into six subsections corresponding to each aspect ratio studied, varying from 10 downwards to 1.1 (except $\chi = 4$ and 5 treated in a common subsection). For each aspect ratio we provide a state diagram in the two-parameter G–m^* plane (figures 1, 4, 6, 9, 11 and 12). The used symbols are listed in table 2. Their choice respects the symbols used in the IJMF paper by Zhou & Dušek (2015) and in the Physics of Fluids paper by Chrust *et al.* (2013). Figures illustrating the trajectory styles described already in previous work are not represented. The reader is referred to the papers cited in table 2 for graphic support. For new regimes typical for intermediate aspect ratios, reference to the subsections where they are described is given. The axis scaling had to be adapted to assure an optimal readability. The scaling of the Galileo numbers is logarithmic, i.e. linear in $\log(G)$. The vertical axis is linear in $\log(m^* + 0.1)$. This indication allows anybody to interpolate the position of any point. Moreover, a sufficient number of labelled ticks are provided. The individual two-parameter G–m^* planes have been swept linewise (for constant m^*). Where additional data were needed to delimit the stability domains, supplementary points have been added. The intersections of bifurcation thresholds with the m^*-lines are determined by interpolation within at least one tenth of the Galileo number. In the higher Galileo number domain, where the stability limits are weakly dependent on the Galileo number, the interpolation was done in the m^* direction. In general, the intersections with the alignments of points in the state diagrams are accurate.

3.1. $\chi = 10$

Compared to a nominally infinitely flat body, a homogeneous disk or a infinitely flat spheroid (having a very similar scenario as that of a disk), the effect of finite thickness is already significant for as flat a spheroid as that of aspect ratio 10. This observation is not new, as the significant difference between a very flat cylinders of

https://doi.org/10.1017/jfm.2017.718 Published online by Cambridge University Press

Symbol	Description
+	**Steady vertical** **States of the scenario of a perfect sphere** (see Zhou & Dušek 2015)
▷	**Steady oblique**
▷ (green)	**Low-frequency oblique oscillating**
▽ (green)	**Low-frequency quasi-periodic oblique oscillating**
▷ (yellow)	**High frequency oblique oscillating**
○ (blue)	**Planar zig-zag**
● (blue)	**3D zig-zagging trajectories**
	States of the scenario of a disk (Chrust *et al.* 2013)
○ (dark blue)	**Flutter** Planar 'zig-zagging' motion accompanied by fast oscillations with significant inclination angles (ϕ) typically larger than 30°.
● (dark blue)	**Helical** Purely helical or bi-periodic states resulting from a slow rotation of the symmetry plane (typical for large Galileo numbers at small dimensionless masses.)
□ (green)	**Intermittent** See Chrust *et al.* (2013, figure 14).
▽ (red)	**Tumbling** See Chrust *et al.* (2013, figure 8).
▼ (red)	**Spiral tumbling** See Chrust *et al.* (2013, figure 20).
• (magenta)	**Vertical periodic of small amplitude** (Replace the magenta asterisks of Chrust *et al.* (2013, figure 22).) Fluid modes with very small amplitudes of the solid-body oscillations.
◇ (magenta)	**Chaotic** Denotes all 3D trajectories with more complicated than bi-periodic dynamics.
	States of spheroids of intermediate aspect ratio
▸ (magenta enclosed in yellow)	**Switching of oblique oscillating and vertical periodic in perpendicular directions** (see §§ 3.4 and 3.5)
○ (magenta)	**Vertical periodic of intermediate amplitude** Periodic fluid modes separated from the flutter by a jump of amplitude and frequency for high aspect ratio. At intermediate aspect ratio, the transition between both is progressive and an arbitrary criterion based on the amplitude of inclination angle (ϕ) is used.
∗ (magenta)	**Planar, quasi-periodic** All planar aperiodic states, vertical in the average or oblique.
▷ (magenta)	**Oblique periodic** Planar, periodic, only slightly drifting in the horizontal direction in contrast with oblique oscillating states for which the mean horizontal velocity dominates.

TABLE 2. Description of symbols presented in the state diagrams of various aspect ratios.

https://doi.org/10.1017/jfm.2017.718 Published online by Cambridge University Press

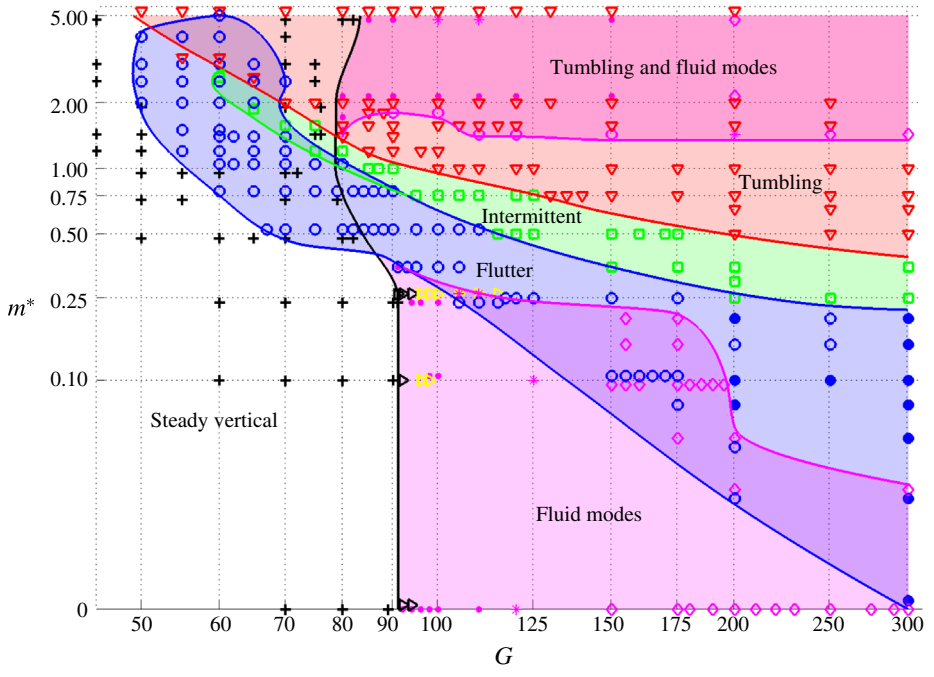


FIGURE 1. (Colour online) State diagram for spheroids of aspect ratio $\chi = 10$. Ticks and labels are not provided for $m^* = 1.2$, 1.4, 1.5 and 1.8 (between 1 and 2) and 2.5, 3 and 4 (between 2 and 5). The three lines between $m^* = 0$ and 0.1 correspond to $m^* = 0.025$, 0.05 and 0.075. A flat, but not infinitely flat, spheroid has a particularly large domain of stability of the flutter (with strongly oscillating trajectories). Small-amplitude fluid modes are present both for small and large inertia. The vertical section of the primary instability threshold is due to the regular bifurcation of the sphere-like scenario.

aspect ratio 10 and a disk was already discussed by Auguste *et al.* (2013). In many experiments, aspect ratios of approximately 10 are considered as representing 'flat' bodies. For this reason $\chi = 10$ can be considered as acceptable starting point of our analysis. There is, indeed, a qualitative resemblance between the state diagram of Chrust *et al.* (2013) and that represented in figure 1. Quantitatively, the differences are, however, significant. In the lower part of the figure ($m^* < 0.3$) we observe an upward shift of the threshold of the primary bifurcation (to $G_{crit} = 91.0$, as compared to less than 80 for the disk) giving rise to 'quasi-vertical' fluid modes. More importantly (unlike for the disk), the primary bifurcation is regular, i.e. the real eigenvalue has become more unstable than the complex eigenpair. This explains why exactly the same critical Galileo number was found for $m^* = 0$, 0.1 and 0.25. The secondary Hopf bifurcation, yielding an oblique oscillating regime, follows at a critical Galileo number slightly above 92. We evidenced oblique oscillating states at $m^* = 0.1$, 0.25 and at $G = 96$, 98. The sequence of these two regimes represents what we decided to call a sphere-like scenario. As the Galileo number increases to 100, the mean value of the horizontal velocity, responsible for the mean horizontal drift, vanishes and a periodically oscillating regime, vertical in the mean, sets in. It is a typical fluid mode with a very weak response of the solid body to flow oscillation. The maximum inclination of the spheroid axis is only a few degrees (see table 3). By restarting using as initial state that obtained at $G = 100$, we verified that at the

https://doi.org/10.1017/jfm.2017.718 Published online by Cambridge University Press

(m^*, G)	$\bar{u}_z$	A_{u_z}	$\bar{u}_h$	A_{u_h}	ϕ_{max} (deg.)	Period
(0.25, 100)	−1.54	0.005	0	0.078	6.1	4.07
(0.25, 115)	−1.38	0.37	0	0.770	49	3.11
(0.75, 200)	−1.33	0.45	0.97	0.32	90	2.18
(2, 65)[a]	−1.41	0.09	0	0.24	50	5.76
(2, 100)[b]	−1.420	0.005	0	0.061	11.1	5.30

TABLE 3. Quantitative data characterizing selected periodic states for aspect ratio $\chi = 10$. $\bar{u}_z$, $\bar{u}_h$ – mean vertical and horizontal velocity, A_{u_z} and A_{u_h} – oscillation amplitudes, ϕ_{max} – maximum inclination angle.

[a]Flutter.
[b]Fluid mode.

Galileo number $G = 96$ the vertical periodic state is not stable. However, at $G = 98$ we found a coexistence of both a vertical and an oblique oscillating state. The same holds for $m^* = 0.25$. For this higher non-dimensionalized mass, the steady oblique state (at $G = 94$) and oblique oscillating states (at $G = 96$, 98, 100 and 105) were found to coexist with the vertical periodic one (at $G = 98$, 100 and 105 they are quasi-periodic). This means that there is no progressive evolution from the steady oblique to vertical periodic regime via an oblique oscillating state (with the mean value tending to vanish progressively). Instead a subcritical bifurcation is at the origin of the vertical periodic state.

It may be objected that this degree of detail might lack physical relevance. The steady oblique and oblique oscillating states might be difficult to evidence experimentally due to their restricted stability domain; however, the independence of the threshold of m^* might be detectable as well as the weakly oscillating vertical trajectories. It is to be noted that the typical Strouhal number of oscillations (based on the mean vertical velocity) is approximately 0.11, as can be inferred from table 3 (first line). This value corresponds rather to that of fluid modes ($St = 0.13$) than solid–fluid modes ($St = 0.05$) of the sphere (see Zhou & Dušek 2015). This justifies not only the choice of the symbols (yellow online) but, more generally, the label 'fluid modes' for the entire lower subdomain (magenta online) of the diagram.

The sphere-like scenario vanishes for $m^* > 0.25$ and at $m^* = 0.5$ the primary bifurcation is clearly subcritical and the scenario of a disk is qualitatively recovered. The domain of coexistence of the flutter (planar zig-zagging trajectory) and of the steady vertical state is extremely large. This is due essentially to the very significant shift of the primary bifurcation threshold to higher Galileo numbers. The lowest threshold, $G_{crit} = 78.0$, was found at $m^* = 1.5$, whereas for infinitely flat spheroid the lowest critical Galileo number was $G_{crit} = 35.3$ (at $m^* = 2$). In contrast, the domain of existence of the flutter did not shrink so much, which results in the large bi-stability domain. The stability domain of the flutter overlaps also with the intermittent and tumbling subdomains, which yields up to three coexisting states for some problem parameters.

Also the tumbling (and partly intermittent) domain extends far leftward (towards lower G) and overlaps with the domain of vertical states. An interesting feature of the scenario, unobserved for disks, consists in the coexistence of the tumbling with small-amplitude periodic and chaotic fluid modes. The stability of fluid modes was also found for aspect ratio infinity, and is due to a smaller moment of inertia of flat

https://doi.org/10.1017/jfm.2017.718 Published online by Cambridge University Press

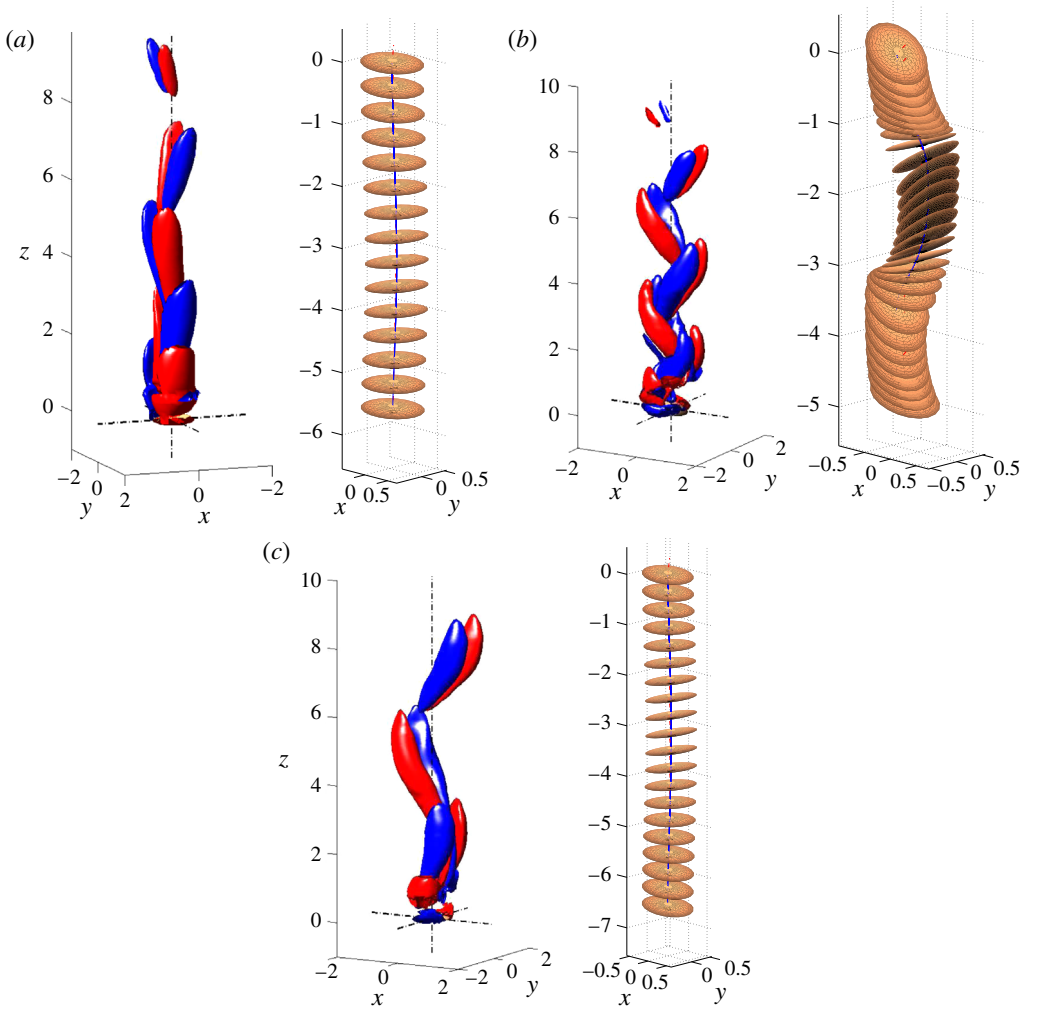


FIGURE 2. (Colour online) Vorticity structures and trajectory of spheroid of aspect ratio 10. (*a*) Vertical periodic state at $m^* = 0.25$, $G = 100$ ($\sin\psi_{max} = 0.1$, vorticity level: $\omega_z = \pm 0.4$), (*b*) flutter at $m^* = 0.25$, $G = 115$ ($\sin\psi_{max} = 0.75$, vorticity level $\omega_z = \pm 0.7$), (*c*) fluid mode at $m^* = 2$, $G = 100$ ($\sin\psi_{max} = 0.19$, vorticity level $\omega_z = \pm 0.7$).

spheroids as compared to disks. Though the zones of their stability are not connected, the fluid modes at high and low inertia present very similar features.

Three types of vertical periodic (zig-zagging) regimes are distinguished in the state diagram 1. To understand their differences, figure 2 represents three examples in terms of the trajectory and streamwise vorticity. The vorticity is about the same both for fluid modes (*a,c*) and the flutter (*b*), while the response of the body to the wake oscillation is very different. In what follows, it will be useful to let quantitative information on the inclination angle appear in the diagrams. Unless otherwise stated, the used criterion for calling the regime 'with intermediate amplitude' and for denoting it by a light (magenta) circle will be a sine of maximum inclination larger than 0.1 and less than 0.4.

https://doi.org/10.1017/jfm.2017.718 Published online by Cambridge University Press

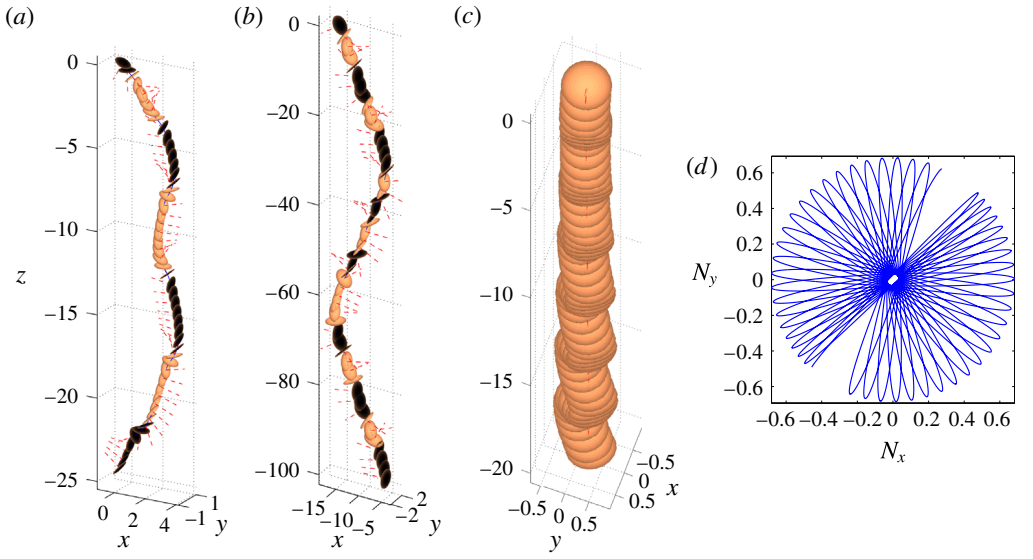


FIGURE 3. (Colour online) 'Intermittent' and helical trajectories of spheroid of aspect ratio 10. (*a*) At $m^* = 0.75$ and $G = 100$; (*b*) at $m^* = 2$ and $G = 65$ (the size of the spheroid is magnified by four in this plot). Kinogram (*c*) and projection of unit vector of the body axis $\boldsymbol{N}$ onto the horizontal plane (*d*) of a trajectory with non-zero helicity at $m^* = 0.1$, $G = 250$.

In the domain of flutter, we evidenced, similarly as for disks, in some cases, a destabilization of the planar trajectories for higher Galileo numbers. The states where this destabilization was positively evidenced are marked by filled circles (blue online) in the diagram of figure 1 and represent trajectories with non-zero helicity. The observed trajectories are, however, not mono-periodic and purely helical-like in the papers by Chrust *et al.* (2013) and Zhong *et al.* (2011). Their projection onto the horizontal plane is rather represented by a turning flat ellipse. As the result, such dynamics is, strictly speaking, quasi-periodic. An example is represented in figure 3(*c*). The kinogram of the motion shows that the trajectory remains actually very close to that of a flutter.

At the interface between the domain of flutter and of tumbling, intermittent states typical for their mostly irregular switching between a zig-zagging (fluttering) stage and tumbling were evidenced in the same way as by Field *et al.* (1997) and Chrust *et al.* (2013), who already noted that, in numerical simulations, the intermittency sometimes becomes periodic with a given number of tumbles alternating in each direction. An example is given in figure 3(*b*) where the body tumbles five times over edge before changing the rotation direction.

3.2. $\chi = 6$

At the primary bifurcation, the state diagram in figure 4 evidences the same early sphere-like scenario as for $\chi = 10$ for small non-dimensionalized masses $m^* \leqslant 0.25$. The primary bifurcation is regular at $m^* \leqslant 0.25$ and its threshold is thus independent of m^* on this interval. The critical Galileo number is 90.1. For this smaller aspect ratio, the transition from the steady oblique to vertical periodic state is progressive,

https://doi.org/10.1017/jfm.2017.718 Published online by Cambridge University Press

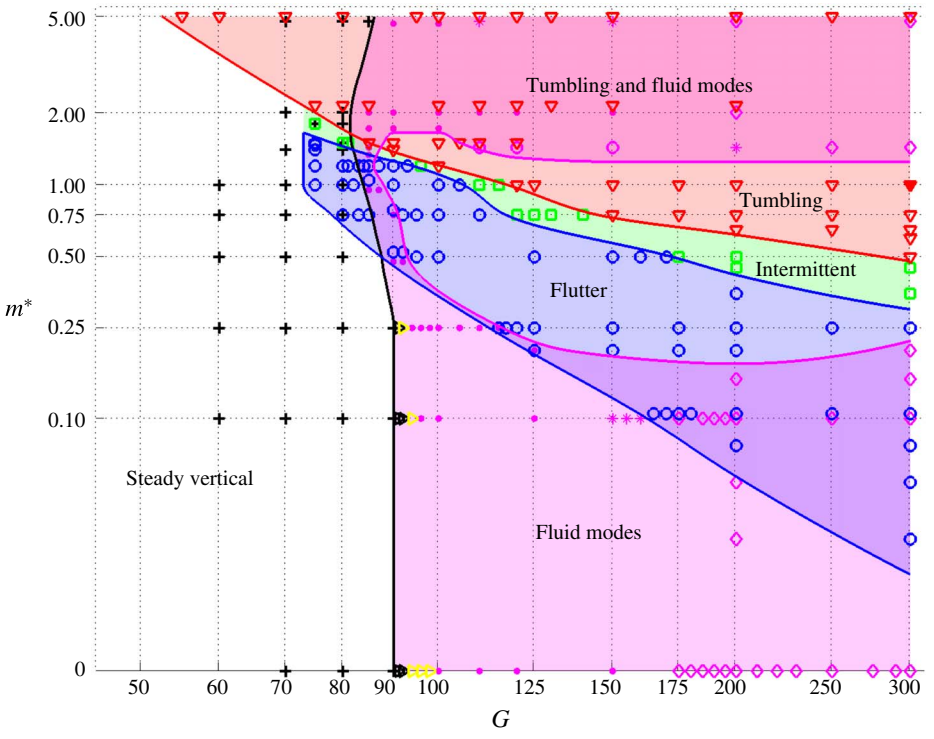


FIGURE 4. (Colour online) The state diagram for spheroids of $\chi = 6$. (The three lines between $m^* = 0$ and 0.1 correspond, again, to $m^* = 0.025$, 0.05 and 0.075.) The domains of flutter and intermittency are smaller as compared to aspect ratio $\chi = 10$.

and there is no bi-stability between the oblique oscillating and vertical periodic fluid mode. In contrast with the $\chi = 10$ aspect ratio, the stability interval of the sphere-like states decreases with increasing m^*.

Unlike for a disk and very flat spheroids of aspect ratios larger or equal than 10, the primary bifurcation is not subcritical at higher non-dimensionalized masses. It continues to be supercritical but of Hopf type, giving rise directly to vertical periodic fluid states. In the interval $0.25 \leqslant m^* < 1.8$, the vertical periodic fluid modes undergo a next bifurcation, which is subcritical and yields states with a significant flutter or directly intermittent or tumbling trajectories. As a result, even in the interval $0.5 \leqslant m^* \leqslant 1.5$ a narrow 'channel' of fluid modes connects the lower area to the upper area, which coexists with tumbling states. This confirms the conjecture formulated in the previous subsection consisting in establishing an analogy between fluid states at small and high inertia. The second bifurcation threshold is marked by the solid light (magenta online) line delimiting the fluid modes from higher Galileo numbers. The stability domain of the flutter extends towards low non-dimensional masses, where it overlaps with fluid modes, and towards small Galileo numbers, where it overlaps, albeit much less than for $\chi = 10$, with the domain of steady vertical trajectories. The progressive transition from a steady vertical regime to flutter with increasing Galileo number is illustrated in figure 5 for $m^* = 1$. The exponential decay of small oscillations of the sine of the inclination angle of body axis at $G = 80$ proves the linear stability of the steady vertical mode. At $G = 85$, the Hopf bifurcation sets in and saturates at

https://doi.org/10.1017/jfm.2017.718 Published online by Cambridge University Press

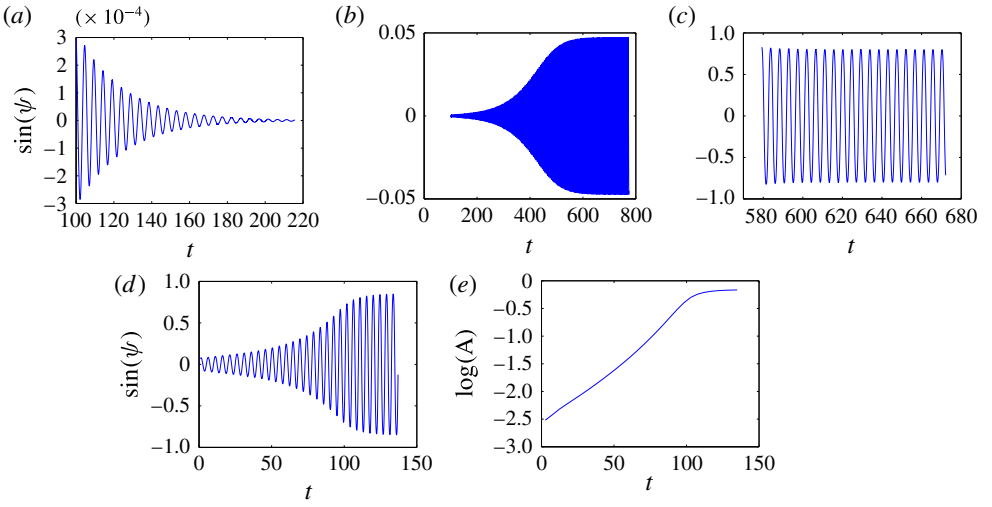


FIGURE 5. (Colour online) Evolution of the inclination of the axis of a spheroid of aspect ratio $\chi = 6$ at $m^* = 1$ and at increasing Galileo numbers. (*a*) $G = 80$: stability of the steady vertical state. (*b*) $G = 85$: convergence to the vertical periodic state with small amplitude of oscillation (fluid mode). (*c*) $G = 85$: Flutter coexisting with the fluid mode at $G = 85$. (*d,e*) $G = 90$: secondary Hopf bifurcation saturating to the flutter. The log of amplitude plot (*e*) demonstrates the subcriticality (see the super-exponential (faster than exponential) growth).

an amplitude less than 0.05 typically for the vertical periodic fluid mode. At $G = 90$ this mode becomes unstable. The new bifurcation is subcritical, as can be seen from the super-exponential growth of the amplitude (figure 5*e*, graph of the logarithm of amplitude at $G = 90$). Panel (*c*) shows the stability of the flutter (sine of inclination of 0.8) at the same Galileo number as that of the fluid mode (panel *b*) at $G = 85$.

The intermittent domain tends to disappear with decreasing aspect ratio. While the subdomain of stability of the tumbling remains roughly the same as for $\chi = 10$, the domain of stability of the flutter gets significantly reduced. It becomes narrower, and the overlapping with vertical regime is much smaller. Obviously, the flutter requires some degree of aerodynamicity while, to sustain the rotating motion in the tumbling regime, the inertia is more important than the shape.

3.3. $\chi = 5$ *and* $\chi = 4$

The differences of the scenario for $\chi = 5$ as compared to $\chi = 6$ can be summed up in the following points (see figure 6).

(i) The regular bifurcation for small m^* is no longer present, i.e. the sphere-like scenario is no longer observed, at least not for $m^* \leqslant 5$. The primary bifurcation is a Hopf one for all non-dimensionalized masses. The critical Galileo number depends on the inertia, albeit rather weakly.

(ii) The trend for the flutter to disappear for smaller aspect ratio continues. Moreover, the separation between fluid and solid modes (flutter) defined by the subcritical bifurcation, yielding a wide overlapping of the stability of both, tends to vanish, too. The jump in amplitude of oscillation and the bi-stability of the flutter and fluid modes is limited only to $m^* \geqslant 0.5$ and Galileo numbers smaller than 110.

https://doi.org/10.1017/jfm.2017.718 Published online by Cambridge University Press

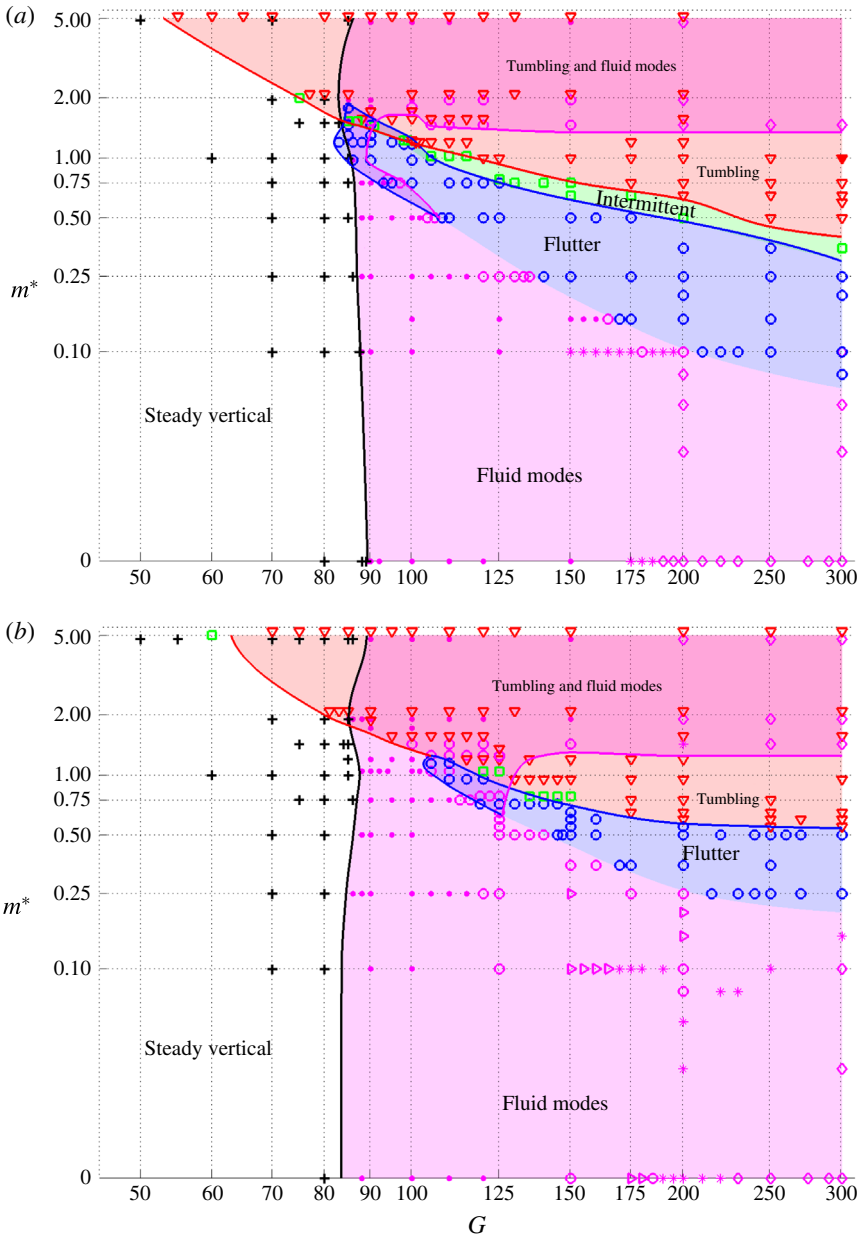


FIGURE 6. (Colour online) State diagrams for spheroids of $\chi = 5$ (*a*) and 4 (*b*). The subcritical bifurcation between the flutter and low-amplitude fluid modes progressively vanishes. At $\chi = 4$, only a small domain of bi-stability of both subsists. The regular primary bifurcation has not been evidenced at these aspect ratios.

This is illustrated by figure 7 showing that, at $m^* = 0.75$ there is a bi-stability between large amplitude (flutter) and small amplitude (fluid mode), at $m^* = 0.5$ there is still a jump, while at $m^* = 0.25$ the amplitude grows continuously with Galileo number. The flutter overlaps only very little with the vertical states.

https://doi.org/10.1017/jfm.2017.718 Published online by Cambridge University Press

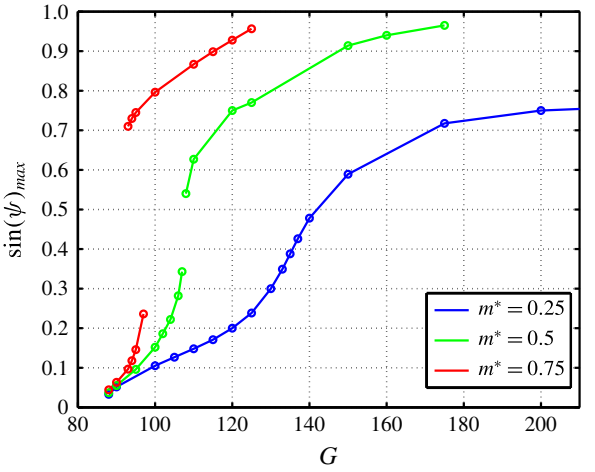


FIGURE 7. (Colour online) Amplitude of the sine of the inclination angle (ψ) as a function of Galileo number for spheroids of aspect ratio $\chi = 5$ and non-dimensionalized masses $m^* = 0.25,\ 0.5$ and 0.75.

(m^*, G)	$\bar{u}_z$	A_{u_z}	$\bar{u}_h$	A_{u_h}	ϕ_{max} (deg.)	Period
(0.1, 100)	−1.56	0.002	0	0.03	3.96	4.88
(0.25, 110)	−1.52	0.003	0	0.05	5.93	4.48
(0.25, 115)	−1.42	0.088	0	0.31	34.92	3.46
(1, 75)	−1.39	0.091	0	0.24	41.96	4.58
(1.5, 150)	−1.47	0.008	0	0.087	18.71	4.51
(2, 150)[a]	−1.39	0.18	0.80	0.12	90	5.26
(2, 150)[b]	−1.48	0.002	0	0.052	11.0	4.60

TABLE 4. Quantitative data characterizing selected periodic states for aspect ratio $\chi = 6$. Same meaning of symbols as in table 3.

[a]Tumbling (period corresponding to a full rotation by 2π).
[b]Fluid mode.

Seen at a constant Galileo number, the evolution from fluid modes to tumbling is progressive, starting from $G > 125$. The amplitude of the inclination angle progressively approaches 90° before tumbling sets in. Since there is no longer any bifurcation between the solid and fluid modes, the distinction between them has been set more or less arbitrarily to $\sin\psi_{max} = 0.4$ in figure 6 (slightly darker grey shade or light blue online for 'flutter'). The chosen value corresponds roughly to the inflection point of the dependence on G.

(iii) The coexistence of the flutter with steady vertical fall vanished between $\chi = 5$ and 4. At $\chi = 4$, the subcritical bifurcation leading to flutter from fluid modes was evidenced only at $m = 0.75,\ 1$ and 1.2.

(iv) The domain of intermittence becomes very narrow and tends to vanish. At aspect ratio $\chi = 4$ (figure 6*b*), only a few intermittent states bordering the tumbling domain were evidenced.

(v) In contrast again, the stability domain of the tumbling remains unaltered.

https://doi.org/10.1017/jfm.2017.718 Published online by Cambridge University Press

(m^*, G)	$\bar{u}_z$	A_{u_z}	$\bar{u}_h$	A_{u_h}	ϕ_{max} (deg.)	Period
(0, 100)	−1.48	0.007	0	0.14	13.08	4.45
(1, 100)	−1.57	0.0009	0	0.024	4.85	5.03
(1, 125)	−1.56	0.005	0	0.056	11.94	4.57
(1, 150)[a]	−1.67	0.3	0.85	0.16	90	5.6
(1, 150)[b]	−1.56	0.012	0	0.084	17.1	4.38
(5,70)[a]	−1.79	0.12	0.45	0.07	90	12.3

TABLE 5. Quantitative data characterizing selected periodic states for aspect ratio $\chi = 3$. Same meaning of symbols as in table 3.

[a]Tumbling.
[b]Fluid mode.

3.4. $\chi = 3$

Two remarkable features distinguish the spheroid of aspect ratio 3 from flatter shapes: the total disappearance of the flutter and the reappearance of the sphere-like states on the side of high inertia.

The flutter, which could be distinguished, at least partially, by a discontinuity from fluid modes at higher aspect ratios, has completely disappeared. Not only is the subcritical bifurcation separating the fluid and solid modes no longer evidenced, but, moreover, as can be seen in table 5, no vertical periodic state has an amplitude of inclination of the body axis exceeding 20° (sine larger than 0.35). All oscillating trajectories are thus fluid modes.

In the absence of a large amplitude of inclination of the zig-zagging states, the tumbling switches directly to a vertical periodic state with only small or intermediate amplitudes of inclination at boundary of the tumbling stability domain. At this aspect ratio, there still subsists a subdomain where the tumbling does not coexist with the fluid mode. At its boundary the fluid mode switches directly to tumbling. For example, the maximum inclination angle of the vertical periodic state at $m^* = 1$ and $G = 195$ is 19°, while at $G = 200$ this state is no longer stable and evolves to tumbling. Similarly, the state $m^* = 1$, $G = 125$ situated very close to the lower boundary of the tumbling stability domain has an inclination amplitude of only 12° (see table 5). At this boundary, three cases of intermittent behaviour changing the sense of rotation have also been evidenced.

The primary instability threshold is that of a Hopf bifurcation for $m^* < 3$ only. At $m^* = 3$, 4, 5 we evidenced a regular bifurcation and a steady oblique primary bifurcating state, making the threshold inertia independent. The m^*-independent critical Galileo number ($G_{crit} = 90.6$) stays remarkably close to that found at $\chi = 10$ and 6. The secondary bifurcation is of Hopf type, leading to the oblique oscillating states typical for the sphere-like scenario. The specificity of its transition to the vertical periodic state (observed also $\chi = 2$) consists in its intermittent character (see figure 8). Instead of saturating to yield a constant non-zero mean, the amplitude grows until the mean value vanishes and a vertical periodic state appears. The latter is not stable either. A steady oblique state in the perpendicular direction arises and the selection of the new symmetry plane of the wake makes the oscillation in the previous direction vanish. The steady oblique state grows until oblique oscillations appear and the cycle repeats regularly. It can be expected that in presence of sufficient random noise the repetition would not be periodic, but rather intermittent. In the example of figure 8, it

https://doi.org/10.1017/jfm.2017.718 Published online by Cambridge University Press

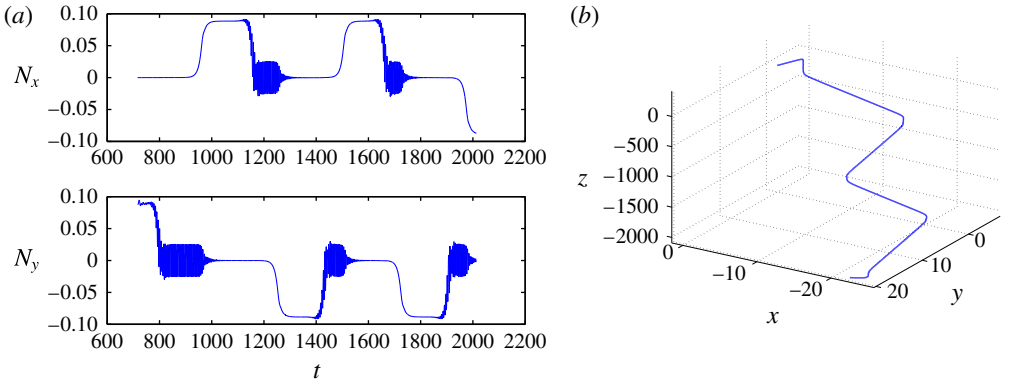


FIGURE 8. (Colour online) $\chi = 3$, $m^* = 5$, $G = 105$: example of a trajectory switching periodically from a vertical periodic to steady oblique and oblique oscillating state. (*a*) Horizontal projections N_x, N_y of the unit vector of the body axis as a function of time, (*b*) trajectory.

can also be seen that the direction of the steady oblique growth in the perpendicular plane is selected arbitrarily. The frequency of oscillation varies only slightly (by less than 10 %) over the whole cycle. The typical Strouhal number is 0.11, i.e. the same as for the oblique oscillating state existing for small inertia at aspect ratio $\chi \geqslant 6$.

3.5. $\chi = 2$

The primary supercritical Hopf bifurcation was evidenced only up to $m^* \leqslant 0.25$ for this aspect ratio. For $m^* \geqslant 0.5$, the primary bifurcation is already regular and the sphere-like scenario sets in at the first two bifurcations. The m^*-independent critical Galileo number is 94.3. The secondary, Hopf bifurcation leads systematically to the already described switching between steady oblique, oblique oscillating and vertical periodic states (see figure 10). The fast frequency corresponds to a Strouhal number of 0.12. The period of the switching is very long, and varies significantly with distance from the instability threshold (more than 1000 at $m^* = 2$, $G = 120$, and approximately 130 at $G = 130$ in figure 10(*c*)), but stays remarkably constant.

We evidenced no mono-stable tumbling subdomain for the aspect ratio 2. Table 6 shows that, again, no vertical periodic state has an amplitude of inclination of the body axis exceeding 20°. Given the absence of mono-stable tumbling, there is no continuous transition from a vertical periodic state to tumbling possible by letting the Galileo number and/or the non-dimensionalized mass numerically evolve. This might mean that a simple acceleration from rest will not yield tumbling unless the rotation is externally triggered. Then the rotation will, however, remain self-sustained. At the edge of the domain of stability of the tumbling mode we still evidenced several cases of intermittent behaviour (squares, green online). Table 6 provides additional quantitative data.

To sum up, periodic vertical trajectories with small to moderate inclination dominate the scenario. Only dense bodies can tumble provided the tumbling is externally triggered.

https://doi.org/10.1017/jfm.2017.718 Published online by Cambridge University Press

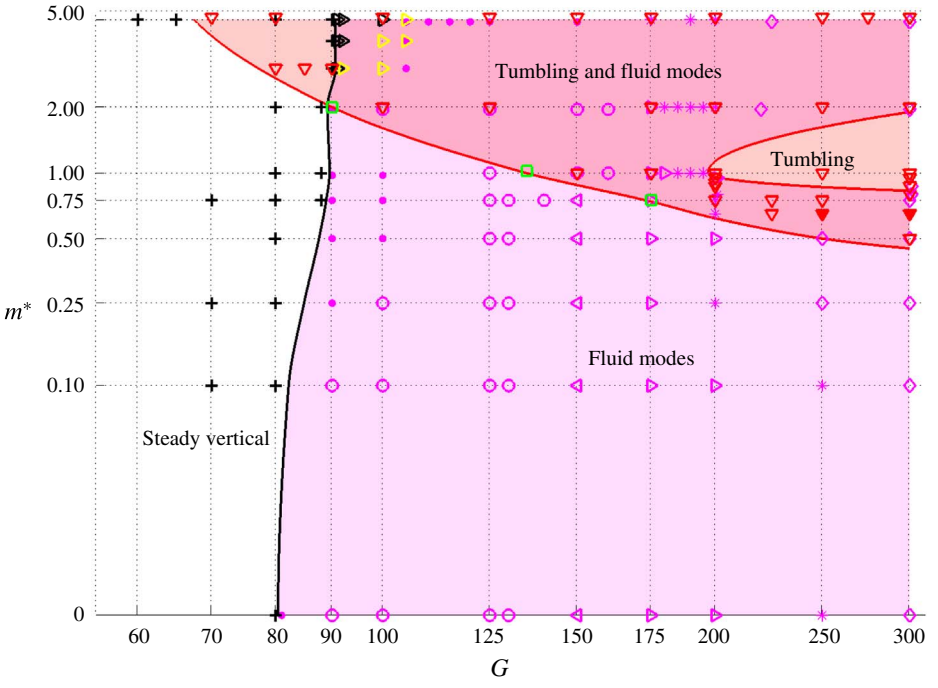


FIGURE 9. (Colour online) The state diagram for spheroids of $\chi = 3$. No flutter has been evidenced. The inclination angle does not exceed 20°. The shape is neither aerodynamic enough nor close to spherical enough to sustain large oscillations. The sphere-like scenario appears at high inertia. There subsists a small mono-stable tumbling subdomain tending to vanish with decreasing aspect ratio as can be seen at $\chi = 2$.

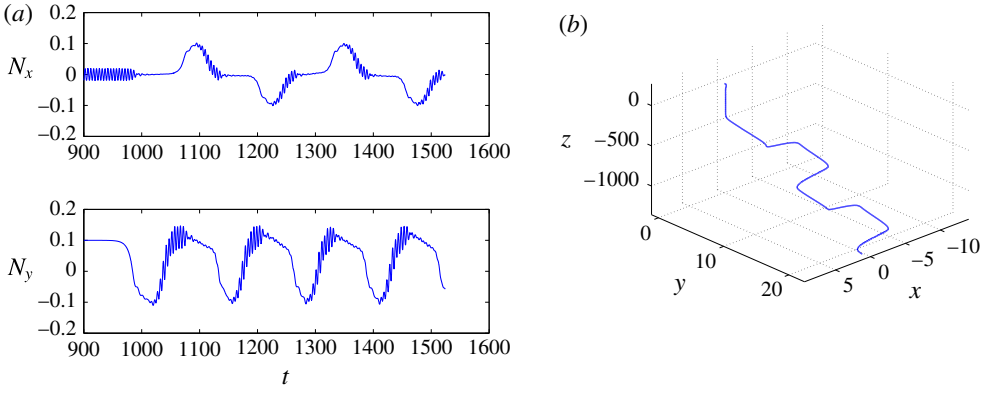


FIGURE 10. (Colour online) $\chi = 2$, $m^* = 5$, $G = 120$: (*a*) Horizontal projections N_x, N_y of the unit vector of the body axis as function of time, (*b*) trajectory.

3.6. $\chi = 1.1$

The transition scenario of a spheroid of aspect ratio $\chi = 1.1$ is close to that of a sphere, but only for sufficiently dense spheroids. The symbols and colours (online) used in figure 12 correspond to those in figure 3 of Zhou & Dušek (2015). The present

https://doi.org/10.1017/jfm.2017.718 Published online by Cambridge University Press

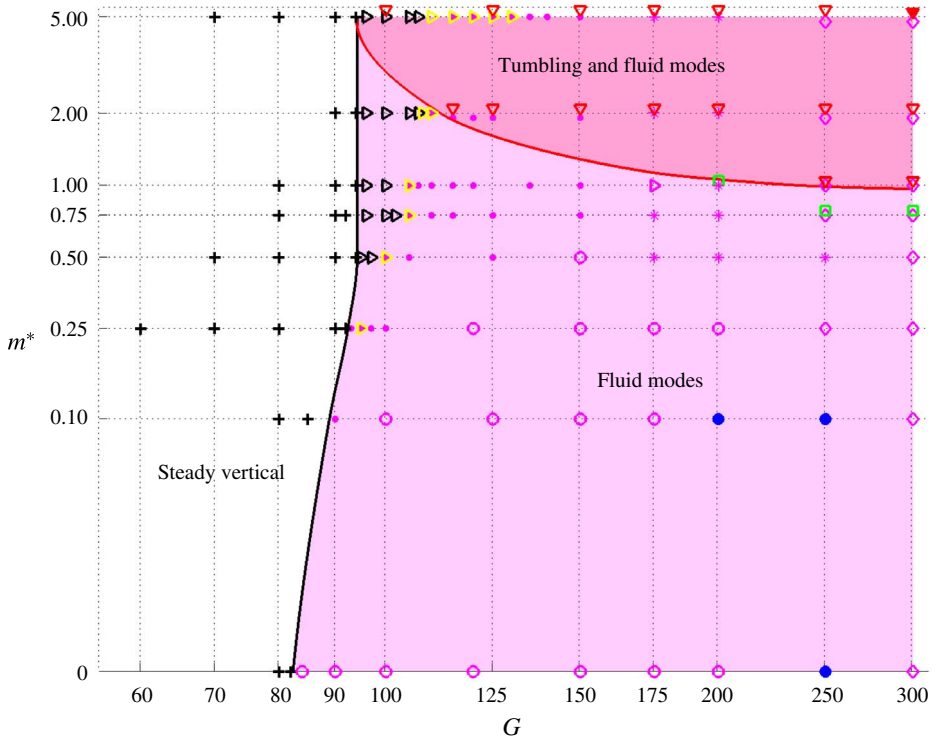


FIGURE 11. (Colour online) The state diagram for spheroids of $\chi = 2$. Unlike at $\chi = 3$, tumbling always coexists with fluid modes. The sphere-like scenario extends towards smaller inertia ($m^* = 0.5$).

(m^*, G)	$\bar{u}_z$	A_{u_z}	$\bar{u}_h$	A_{u_h}	ϕ_{max} (deg.)	Period
(0.1, 100)	−1.53	0.017	0	0.23	16.48	5.28
(0.5, 150)	−1.65	0	0	0.13	12.07	4.73
(1, 150)	−1.68	0	0	0.072	11.24	4.64
(2, 150)[a]	−1.75	0.13	0.77	0.053	90	3.71
(2, 150)[b]	−1.72	0	0	0.046	12.75	4.72

TABLE 6. Quantitative data characterizing selected periodic states for aspect ratio $\chi = 2$. Same meaning of symbols as in table 3.

[a]Tumbling.
[b]Fluid mode.

case of almost spherical body can be quantitatively compared to a perfect sphere by converting the non-dimensionalization. If we neglect the small difference of aspect ratio, the present definition of the non-dimensionalized mass differs by a factor $\pi/6$ from the density ratio ($m^* = \pi/6\,\rho_s/\rho$), and the reference velocity (2.2) differs from that used for the perfect sphere (see (3) of Zhou & Dušek 2015) by a factor $\sqrt{\pi/6}$ (i.e. $U_{ref} = \sqrt{\pi/6}\,U_{ref,sphere}$). As the result, the Galileo number defined by (1.1) is smaller by this factor and the velocities and frequencies are larger by its inverse. The primary bifurcation threshold (that of the steady oblique regime) found to be

https://doi.org/10.1017/jfm.2017.718 Published online by Cambridge University Press

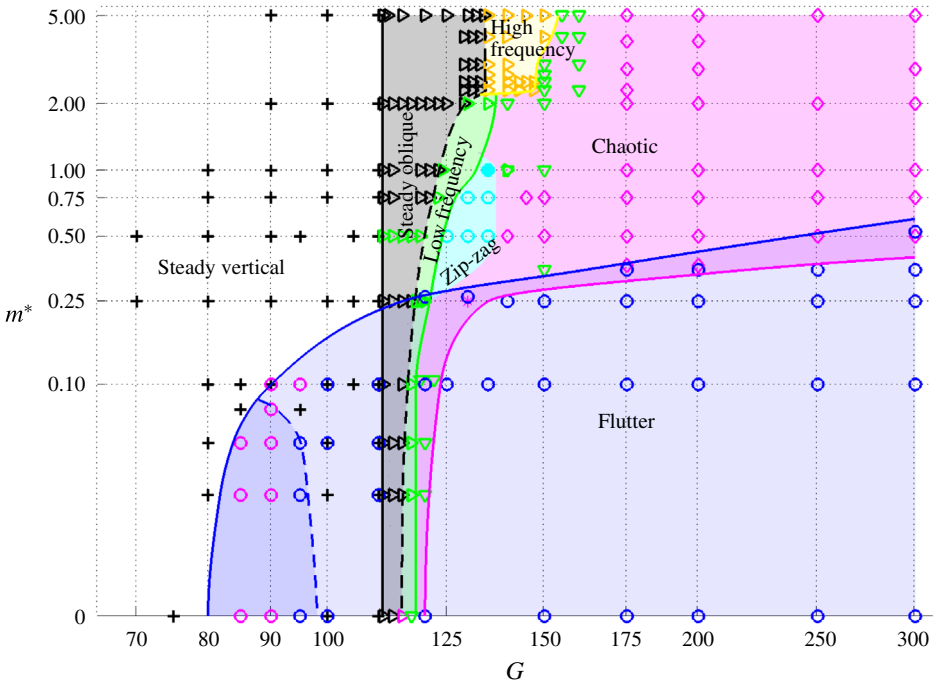


FIGURE 12. (Colour online) The state diagram for spheroids of $\chi = 1.1$. For $m^* > 0.25$, i.e. density ratio larger than 0.5, the spheroid behaves qualitatively like a perfect sphere. Trajectories of very light spheroids are zig-zagging with large amplitude of inclination angle allowed by the almost spherical shape.

$G^*_{crit} = 155.8$ (independently of the density ratio) becomes $G_{crit} = 112.7$ in terms of the definition (1.1). For an almost spherical spheroid of aspect ratio $\chi = 1.1$, this threshold lies at $G_{crit} = 110.8$ and is represented by the black vertical line separating the domain of steady vertical trajectories (black crosses) from that of steady oblique regimes (rightward pointing black triangles). It is to be noted that, unlike the perfect sphere, the spheroid does not rotate. This fact has a very limited impact on the onset of the primary instability and on the whole scenario for sufficiently dense bodies, i.e. for $m^* > 0.25$ and density ratios larger than 0.5 For the assessment of quantitative agreement and differences see the top part of table 7. It is also interesting to compare figure 12 with the corresponding state diagram in figure 3 of Zhou & Dušek (2015).

In contrast to this close similarity to the scenario of a perfect sphere for higher non-dimensionalized masses, the diagram of figure 12 presents features typical for flat bodies for very small inertia (m^* roughly smaller than 0.25). We evidenced a bounded area of linear instability below the threshold of the steady oblique regime for $m^* < 0.1$ and $80 \leqslant G < 10$. In figure 12, the area is delimited by a solid (blue online) line from lower Galileo numbers and by a dashed (blue) line from higher Galileo numbers, and is filled in a darker colour. The solid and dashed lines correspond, for increasing Galileo numbers at constant m^*, respectively, to a destabilization and re-stabilization of the vertical trajectory. The lines determine the threshold of the Hopf bifurcation yielding a planar oscillating trajectory, vertical in the average (zig-zagging trajectory). The frequency is slightly higher than the low frequency of the oblique oscillating regime for similar inertia: 0.12 to 0.14 as compared to 0.10.

https://doi.org/10.1017/jfm.2017.718 Published online by Cambridge University Press

Spheroid of aspect ratio $\chi = 1.1$ and sphere								
(m^*, G)	u_z	u_h	A_{u_h}	$\sin\psi$	$A_{sin\psi}$	f	Ω_h	A_{Ω_h}
(0.25,115)	1.81	0.098	0	0.078	0	Steady		
(0.26, 116)	1.83	0.088	0			Steady	0.016	0
(0.25,120) (oo)	1.83	0.12	0.046	0.090	0.042	0.096		
(0.26, 126)	1.86	0.15	0.043			0.087	0.020	0.013
(0.5,130) (zz)	1.86	0	0.25	0	0.21	0.043		
(0.26,130)	1.86	0	0.27			0.033	0.054	
(1,120)	1.83	0.133	0	0.101	Steady			
(1.05,123)	1.85	0.146	0			Steady	0.015	0
(2.5,140) (oohf)	1.89	0.185	0.0029	0.122	0.0007	0.24		
(2.1,145)	1.92	0.196	0.0026			0.25	0.010	0.0006
(2,300)[a]	2.15	0.03	0.14	0.01	0.10	0.08		
(2.1,270)[a]	2.16	0.03	0.11			0.09	0.006	0.018
Vertical oscillating states of spheroid $\chi = 1.1$								
(m^*, G)	u_z	u_h	A_{u_h}	$\sin\psi$	$A_{sin\psi}$	f		
(0.025, 90)	1.62	0	0.31	0	0.34	0.13		
(0.025, 110)	1.61	0	0.49	0	0.56	0.14		
(0.35,175)	1.76	0	0.60	0	0.78	0.124		
(0.35,175)[a,b]	1.95	0	0.19	0	0.19	0.095		

TABLE 7. Top: comparison of some characteristic regimes of a spheroid of aspect ratio $\chi = 1.1$ (upper lines) and of a sphere (lower lines). oo – oblique oscillating, *zz* – low-frequency periodic zig-zagging, oohf – oblique oscillating, high frequency. (Parameters relevant for the sphere are converted to the non-dimensionalization of the present paper.) u_h: (average) horizontal velocity, A_{u_h}: horizontal velocity amplitude, $\sin\psi$: (average) sine of inclination, $A_{sin\psi}$: amplitude of oscillations of the body axis in terms of the sine of inclination, f: frequency, Ω_h: (average) horizontal projection of angular velocity, A_{Ω_h}: amplitude of Ω_h. Bottom: characteristics of some vertical oscillating states of spheroid of $\chi = 1.1$.

[a]Non-periodic states – amplitudes replaced by r.m.s. and frequency by the peak of power spectrum corresponding to the most visible oscillations.
[b]Coexisting chaotic sphere-like state.

At saturation, the oscillations of the body are (unlike the fluid modes discussed elsewhere) significant. Though, in this case, there is no physical reason to distinguish 'small' angles of inclination of the axis from larger ones, we keep the notation of table 2 and set the distinction at 24° (sine equal to 0.4). This enables us to show that most vertical oscillating states have a larger inclination amplitude. For this reason we label the subdomain as 'flutter' (though the idea of flutter does not really apply to the present thick shape). The amplitude of inclination reaches almost 90° at $G = 300$, in agreement with the expectation that for higher Galileo the spheroid will start to rotate (tumble) in the same way as a perfect sphere. The lighter grey (magenta online) symbols indicating smaller amplitudes than 24° are confined to the proximity of the threshold where the bifurcation is supercritical and the amplitude increases theoretically from zero. In spite of that, even these represented states have inclination angles of at least 12°. The bifurcation corresponding to the re-stabilization

https://doi.org/10.1017/jfm.2017.718 Published online by Cambridge University Press

is subcritical. As a result, the flutter remains stable outside the described small subdomain of linear instability of the vertical ascension. The domain of stability of this regime partially coexists with the states characteristic for a spherical body; however, this overlapping is very limited and the oscillations obviously kill the chaotic regimes found for a perfect sphere. We did not find any coexisting chaotic regimes in the lower right corner of the diagram delimited roughly by $m^* < 0.25$ and $G > 125$.

Perfect spheres with little inertia have been shown to describe mostly chaotic trajectories for higher Galileo numbers except for an 'island' of vertical oscillating trajectories situated around the parameter point (in the present non-dimensionalization) $m^* = 0.5$, $G = 200$. The frequency of oscillation at this point was found to be 0.2 (in the present non-dimensionalization). The spatial amplitude of oscillation about the vertical direction is very small for this state – approximately 0.1 of the sphere diameter so that these trajectories may be appropriately called 'quasi-vertical'. At a close point $m^* = 0.25$, $G = 200$, the trajectory of the spheroid of aspect ratio 1.1 presents completely different characteristics. The oscillation frequency is 0.125 (instead of 0.2) and the amplitude of excursions with respect to the vertical direction is equal to $1d$. This shows that the flutter of the spheroid has nothing to do with the periodic quasi-vertical regime of a perfect sphere.

The trajectories of slightly flattened spheres (spheroids of aspect ratio 1.1) are reminiscent of the 'vibrating regimes' described by Horowitz & Williamson (2010). For Reynolds numbers smaller than 1550 these regimes were found to be delimited by a density ratio 0.36 and $Re = 260$. This corresponds to $m^* = 0.19$ and $G \approx 160$ in terms of our parametrization and with account of the mean vertical velocity remaining close to 1.6. The trajectories were found very accurately periodic. At $Re = 450$ and density ratio 0.11, the amplitude of horizontal excursions was found to be $1d$ and the vertical wavelength of $14d$. At $m^* = 0.1$ and $G = 250$, we find an amplitude of $0.96d$ and wavelength $11.5d$. The vibrating modes were shown to yield a larger mean drag coefficient ($C_D \approx 0.8$) than modes with 'rectilinear trajectories' (having a drag coefficient close to that of a fixed sphere). We find $C_D \approx 0.9$ in our domain of 'flutter', while at a similar Reynolds number (400) in the 'chaotic' domain of a perfect sphere (at $m^* = 0.5$ and $G = 200$), C_D is equal to 0.66. The agreement with the observations of Horowitz & Williamson (2010) is striking, whereas the simulation of the motion of perfect homogeneous spheres in Zhou & Dušek (2015) failed to yield any resemblance.

4. Conclusion and discussion

In the present paper we investigated the effect of aspect ratio on the transition scenario of oblate spheroids. The intention was to provide a link between the known results, those relative to perfect homogeneous spheres and to homogeneous infinitely flat discs. The investigation of the three-parameter space was conducted in parameter planes of constant aspect ratio. This choice is, of course, arbitrary and the parameter space might have been swept differently depending on the application. E.g. for spheroids manufactured of the same material and investigated in the same fluid, a $\rho_s/\rho = \text{const.}$ parameter plane would be of interest. Due to the fact that the definition of the non-dimensionalized mass mixes both the density and aspect ratios, this plane results in a non-trivial surface in the present parametrization. For some purposes, the number of $\chi = \text{const.}$ planes might thus be insufficient. Nevertheless, we hope that not only the investigation of individual $\chi = \text{const.}$ planes has been carried out sufficiently in detail but that the spacing between the aspect ratios is not too coarse

https://doi.org/10.1017/jfm.2017.718 Published online by Cambridge University Press

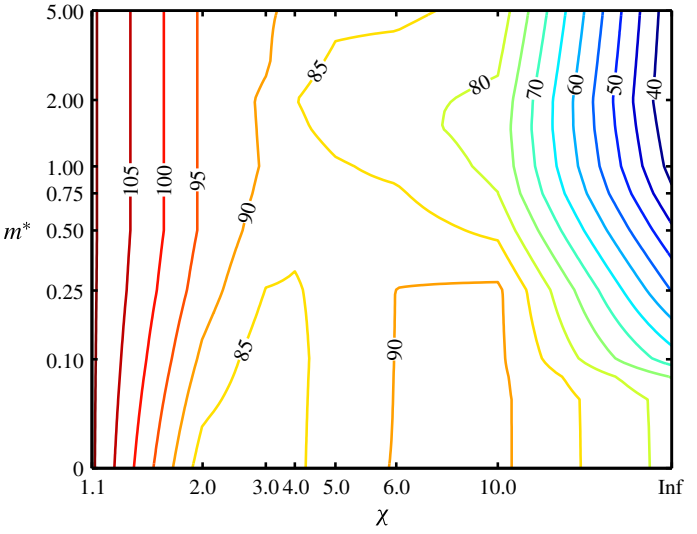


FIGURE 13. (Colour online) Critical Galileo number of the primary instability as a function of the aspect ratio and non-dimensionalized mass. The horizontal axis is linear as a function of $\xi = 1/(1+\chi)$ and the vertical axis as a function of $\mu = \log_{10}(m^* + 0.05)$.

to prevent a potential user of our results from a reliable interpolation. The generated time series can be provided on demand by the corresponding author.

The critical Galileo number of the primary instability threshold can be represented as a function of two variables in the χ–m^* plane. This comprehensive information is represented in figure 13. The straight vertical isocontours facilitate the localization of the discussed sphere-like scenario, present for flat and thick spheroids.

The scenario is strongly marked by subcritical effects making sometimes several totally different regimes coexist for the same set of parameters. This opens the problem of receptivity in experimental applications where noise is never absent. The numerical reproducibility of results might depend on the choice of initial conditions. The two basic regimes of falling disks – the flutter and the tumbling – remain of importance throughout the whole scenario. Especially the robustness of the tumbling, evidenced down to the aspect ratio of 2, is remarkable. The separation between 'flat' and 'thick' spheroids lies between $\chi = 3$ and 4 and can be defined by the disappearance of the flutter, i.e. of vertical periodically oscillating trajectories with large inclination angles of the body. A similar qualitative limit was found for fixed spheroids and cylinders placed in a uniform flow (see Chrust *et al.* 2010). In contrast, the tumbling regime is stable for all aspect ratios larger or equal than 2 – i.e. for sufficiently aspherical bodies.

The investigation of the spheroid of aspect ratio 1.1 indicates that the dynamics of massive bodies is relatively robust to geometric imperfection of the body shape and the sphere scenario is qualitatively well reproduced in spite of the absence of rotation of the spheroid. In contrast, very significant oscillations of the body axis for ascending almost spherical spheroids of very low solid/fluid density ratio make the dynamics very different from that of perfect spheres. This might be a hint for the explanation of the zig-zagging trajectories observed by Horowitz & Williamson (2010) that we failed to explain using the results of simulations of freely moving perfect spheres. Obviously, very light spheres are very sensitive to imperfections of all sort

https://doi.org/10.1017/jfm.2017.718 Published online by Cambridge University Press

(see also Jenny *et al.* 2004). More broadly, an ideal spherical body is perhaps not an ideal prototype representing solid bodies of arbitrary shapes.

REFERENCES

AUGUSTE, F. 2010 Instabilités de sillage générées derrière un corps solide cylindrique, fixe ou mobile dans un fluide visqueux. PhD thesis, Université Paul Sabatier, Toulouse.

AUGUSTE, F., MAGNAUDET, J. & FABRE, D. 2013 Falling styles of discs. *J. Fluid Mech.* **719**, 388–405.

CHRUST, M. 2012 Etude numérique de la chute d'objets axisymétriques dans un fluide newtonien. PhD thesis, Université de Strasbourg.

CHRUST, M., BOUCHET, G. & DUŠEK, J. 2010 Parametric study of the transition in the wake of oblate spheroids and flat cylinders. *J. Fluid Mech.* **665**, 199–208.

CHRUST, M., BOUCHET, G. & DUŠEK, J. 2013 Numerical simulation of the dynamics of freely falling discs. *Phys. Fluids* **25**, 044102.

CHRUST, M., BOUCHET, G. & DUŠEK, J. 2014 Effect of solid body degrees of freedom on the path instabilities of freely falling or rising flat cylinders. *J. Fluids Struct.* **47**, 55–70.

ERN, P., RISSO, F., FABRE, D. & MAGNAUDET, J. 2011 Wake-induced oscillatory paths of bodies freely rising of falling in fluids. *Annu. Rev. Fluid Mech.* **44**, 97–121.

FABRE, D., AUGUSTE, F. & MAGNAUDET, J. 2008 Bifurcations and symmetry breaking in the wake of axisymmetric bodies. *Phys. Fluids* **20**, 051702.

FABRE, D., TCHOUFAG, J. & MAGNAUDET, J. 2012 The steady oblique path of bouyancy-driven disks and spheres. *J. Fluid Mech.* **707**, 24–36.

FERNANDES, P. C., RISSO, F., ERN, P. & MAGNAUDET, J. 2007 Oscillatory motion and wake instability of freely rising axisymmetric bodies. *J. Fluid Mech.* **573**, 479–502.

FIELD, S. B., KLAUS, M. & MOORE, M. G. 1997 Chaotic dynamics of falling disks. *Nature* **388**, 252–254.

HOROWITZ, M. & WILLIAMSON, C. H. K. 2010 The effect of Reynolds number on the dynamics and wakes of freely rising and falling spheres. *J. Fluid Mech.* **651**, 251–294.

JENNY, M. & DUŠEK, J. 2004 Efficient numerical method for the direct numerical simulation of the flow past a single light moving spherical body in transitional regimes. *J. Comput. Phys.* **194**, 215–232.

JENNY, M., DUŠEK, J. & BOUCHET, G. 2004 Instabilities and transition of a sphere falling or ascending freely in a Newtonian fluid. *J. Fluid Mech.* **508**, 201–239.

STRINGHAM, G. E., SIMONS, D. B. & GUY, H. P. 1969 *The Behavior of Large Particles Falling in Quiescent Liquids*. U.S. Government Printing Office.

TCHOUFAG, J., FABRE, D. & MAGNAUDET, J. 2014 Global linear stability analysis of the wake and path of buoyancy-driven disks and thin cylinders. *J. Fluid Mech.* **740**, 278–311.

UHLMANN, M. & DOYCHEV, T. 2014 Sedimentation of a dilute suspension of rigid spheres at intermediate Galileo numbers: the effect of clustering upon the particle motion. *J. Fluid Mech.* **752**, 310–348.

UHLMANN, M. & DUŠEK, J. 2014 The motion of a single heavy sphere in ambient fluid: a benchmark for interface-resolved particulate flow simulations with significant relative velocities. *Intl J. Multiphase Flow* **59**, 221–243.

WILLMARTH, W. W., HAWK, N. E. & HARVEY, R. L. 1964 Steady and unsteady motions and wakes of freely falling disks. *Phys. Fluids* **7**, 197–208.

ZHONG, H., CHEN, S. & LEE, C. 2011 Experimental study of freely falling thin disks: Transition from planar zigzag to spiral. *Phys. Fluids* **23** (1), 011702.

ZHOU, W. & DUŠEK, J. 2015 Chaotic states and order in the chaos of the paths of freely falling and ascending spheres. *Intl J. Multiphase Flow* **75**, 205–223.

https://doi.org/10.1017/jfm.2017.718 Published online by Cambridge University Press